Korean J. Chem. Eng., 33(3), 838-843 (2016)
DOI: 10.1007/s11814-015-0240-6

pISSN: 0256-1115
eISSN: 1975-7220

Selective oxidation of H_2S to sulfur over CeO_2-TiO_2 catalyst

Dong-Heon Kang, Moon-Il Kim, and Dae-Won Park†

School of Chemical and Biomolecular Engineering, Pusan National University, Busan 46241, Korea
(*Received 13 August 2015 • accepted 11 November 2015*)

Abstract−The catalytic oxidation of hydrogen sulfide (H_2S) to elemental sulfur was studied over CeO_2-TiO_2 catalysts. The synthesized catalysts were characterized by various techniques such as X-ray diffraction, BET, X-ray photoelectron spectroscopy (XPS), temperature-programmed desorption of ammonia, and scanning electron microscopy (SEM). Catalytic performance studies of the CeO_2-TiO_2 catalysts showed that H_2S was successfully converted to elemental sulfur without considerable emission of sulfur dioxide. CeO_2-TiO_2 catalysts with Ce/Ti=1/5 and 1/3 exhibited the highest H_2S conversion, possibly due to the uniform dispersion of metal oxides, high surface area, and high amount of acid sites.

Keywords: Selective Oxidation, Hydrogen Sulfide, Sulfur, CeO_2-TiO_2 Catalyst

INTRODUCTION

Hydrogen sulfide is a byproduct of fuels in oil, coal, and natural gas reforming processes. It is usually removed by the well-known Claus process, a two-step process including thermal oxidation and catalytic reaction [1,2]. In the first stage, one-third of the initial H_2S is transformed to SO_2 in a combustion chamber at 1,000-1,200 °C

$$H_2S+3/2\ O_2 \rightarrow SO_2+H_2O \quad (1)$$

In the second stage, SO_2 and H_2S are further transformed catalytically into elemental sulfur in a series of reactors, followed by reaction 2.

$$SO_2+2\ H_2S \rightarrow 2\ H_2O+3/n\ S_n \quad (2)$$

However, 3-5% of H_2S could not be converted to S because of thermodynamic limitations [3]. Various commercial processes based on adsorption, absorption, and wet oxidation have been used to treat tail gases containing low concentrations (<5 vol%) of S from Claus plants or other emission sources. Among these processes, dry catalytic oxidation of H_2S to elemental sulfur after the hydrogenation of the S-containing gas to H_2S is a highly promising approach as a result of its thermodynamic completeness.

$$H_2S+1/2\ O_2 \rightarrow 1/n\ S_n+H_2O \quad (3)$$

$$1/n\ S_n+O_2 \rightarrow SO_2 \quad (4)$$

Two commercially developed processes that are based on the direct oxidation of H_2S to elemental sulfur are the Mobil direct oxidation process (MODOP) [4,5] and Super Claus Process [6,7]. The first-generation catalyst used by Super-Claus process is α-alumina supported iron oxide/chromium oxide [7], and the catalyst used by Mobil's direct-oxidation process is a TiO_2-based catalyst [4]. Research continues to obtain a more active catalyst [8].

Vanadium-based catalysts have been reported to be active and selective for the partial oxidation of H_2S to sulfur in the 200-300 °C temperature range [9-16]. In our previous study [17-21], we reported the catalytic performance of vanadia-supported pillared clay for the selective catalytic oxidation of H_2S to elemental sulfur. Many other metal oxides and mixed metal oxides were also studied to develop more efficient catalysts for the vapor phase reaction of H_2S [8,22,23].

Titania (TiO_2) and ceria (CeO_2) have been extensively studied for various applications. TiO_2 is well-known for photocatalysis and environmental catalysis [24,25]. CeO_2 is known as an excellent support for base metals and noble metals in a variety of catalytic processes because of its high oxygen storage capacity, redox properties, and metal-support interactions [26,27]. In addition to pure TiO_2 and CeO_2, modified TiO_2-based and CeO_2-based mixed oxides have attracted much interest for catalytic applications because of their improved properties [28,29]. CeO_2-TiO_2 mixed oxide was studied in various applications, either as support or as catalyst, such as catalytic wet air oxidation reactions of organic compounds [30], NO removal [31] and Diesel soot combustion [32].

Generally, high activity and selectivity of metal oxide supported titania are attributed to the loading and dispersion. The catalysts prepared by a sol-gel method had higher activity and better tolerance to SO_2 than those prepared by an impregnation or coprecipitation method [33]. Therefore, concerning a metal oxide catalyst, a sol-gel method could be an alternative to prepare catalysts with highly dispersed species and nano-scale oxides in the structure [34].

In this study, we report the preparation of CeO_2-TiO_2 catalysts by sol-gel method. The synthesized materials have been characterized and their catalytic performance in the selective oxidation of H_2S has been investigated.

EXPERIMENTAL

1. Preparation of Catalyst

TiO_2 and CeO_2-TiO_2 catalysts were prepared by a sol-gel method reported previously [35]. The volumetric ratio of tetrabutylorthoti-

†To whom correspondence should be addressed.
E-mail: dwpark@pusan.ac.kr
‡This article is dedicated to Prof. Seung-Il Woo on the occasion of his retirement from KAIST.

tanate ($Ti(OC_4H_9)_4$, A.R.), deionized water, anhydrous ethanol (C_2H_5OH, A.R.) and HNO_3 (A.R.) was 1 : 1 : 5 : 0.2. First, $Ti(OC_4H_9)_4$ and anhydrous ethanol were uniformly mixed with a volumetric ratio of 1 : 4. Anhydrous ethanol, deionized water and HNO_3 were mixed, and then $Ce(NO_3)_3{\cdot}6H_2O$ was uniformly dissolved into the ethanolic aqueous solution. Second, the $Ti(OC_4H_9)_4$/ethanol solution was added dropwise to the ethanolic solution at room temperature under strongly stirring to carry out hydrolysis. After continuous stirring for 3 h, the yellowish transparent sol was obtained. Finally, the sol was dried at 80 °C for 24 h to give xerogel. The powder of the xerogel was calcined under air at 500 °C for 3 h to obtain TiO_2 and CeO_2-TiO_2 catalysts. The atom ratio of Ce and Ti is 5/1, 3/1, 1/1 and 1/3, respectively. CeO_2 catalyst was prepared with coprecipitation by adding dropwise 0.2 M $Ce(NO_3)_3$ aqueous solution to excess ammonia solution. The precipitate was dried at 100 °C for 12 h and calcined under air flow at 500 °C for 3 h to get CeO_2 catalyst.

2. Characterization of Catalysts

The chemical composition of the samples was determined by X-ray fluorescence (XRF, Philips PW 2400) and inductively coupled plasma optical emission spectroscopy (ICP-OES, JOBIN YVON). The X-ray diffraction (XRD) patterns were obtained on a Bruker Advanced D8 powder diffractometer using Ni-filtered Cu Kα radiation (λ=1.5404 Å). A fixed power source (40 kV, 300 mA) and a scan speed of 0.02° 2θ min^{-1} were applied to determine the XRD patterns.

The surface areas were determined by N_2 adsorption at 77 K using a Micromeritics ASAP 2010 instrument. Prior to N_2 adsorption, the samples were outgassed under vacuum for 12 h at 110 °C. The specific surface areas were calculated using the BET equation, and the total pore volumes were evaluated from the N_2 uptake at a relative pressure of P/P_0=0.99.

X-ray photoelectron spectroscopy (XPS) analyses were performed using an X-ray photoelectron spectrometer (VG, ESCALAB 250) with monochromatic Al Kα radiation (hυ=1486.6 eV). The samples were calcined at 400 °C for 3 h and pressed into self-supporting wafers without a binder; they were then pretreated under an ultrahigh vacuum. The binding energies (BE) were calculated using C 1s as the reference (284.6 eV) band.

Temperature-programmed desorption of ammonia (NH_3-TPD) was performed with a BEL-CAT chemisorption apparatus (BEL, JAPAN). For NH_3-TPD, approximately 50 mg of the sample was pretreated at 400 °C for 2 h under He flow and was cooled to ambient temperature. Pure NH_3 gas (50 mL/min) was adsorbed at 100 °C for 20 min. Desorption involved a linear heating rate of 10 °C/min at a He flow rate of 20 mL/min. Transmission electron microscopy (TEM) analysis was performed using a JEOL 2011 electron microscope fitted with a lanthanum hexaboride (LaB_6) filament and operated at 200 kV.

3. Reaction Tests

The reaction tests were in a continuous flow fixed-bed reactor made from a Pyrex tube with 1-inch internal diameter. A gaseous mixture of H_2S, O_2, and a balance of He (purity of 50%, 99.9%, and 99%, respectively) was used. To condense the solid product (S), a condenser was attached to the effluent side of the reactor and its temperature was maintained at 110 °C. A line filter was installed after the condenser to trap any solid mist not captured by the condenser. All the lines and fittings from the condenser to the gas chromatograph (GC) were heated above 120 °C to prevent condensation of the water vapor. The gas flow rate was controlled using mass flow controllers (Brooks MFC, 5850E). In a typical experiment, the reactant composition consisted of 5 vol% H_2S, 2.5 vol% O_2, and the remaining composition consisted of He. The gas hourly space velocity (GHSV) was fixed at 10,000 h^{-1}.

The content of the effluent gas was analyzed by a GC (HP 5890) containing a 1.8-m Porapak T column (80-100 mesh) equipped with a thermal conductivity detector at 100 °C. The exit gas from the analyzer was passed through a trap containing concentrated NaOH solution and was vented to a hood. The % conversion of H_2S and the % selectivity toward SO_2 and S are defined as follows:

$$\text{Conversion of } H_2S = \frac{[H_2S]_{inlet} - [H_2S]_{outlet}}{[H_2S]_{inlet}} \times 100(\%)$$

$$\text{Selectivity to a special product } (SO_2, S) = \frac{[\text{Product}]_{outlet}}{[H_2S]_{inlet} - [H_2S]_{outlet}} \times 100(\%)$$

RESULTS AND DISCUSSION

1. Characterization of Catalysts

Fig. 1 shows the high-angle XRD patterns of CeO_2-TiO_2, TiO_2, and CeO_2. For TiO_2 and low Ce loading CeO_2-TiO_2, only anatase TiO_2 peaks (2θ=25.2, 37.9, 47.9°) are observed. As the Ce loading increased, the diffraction lines of TiO_2 became faint and broader, while those of CeO_2 (2θ=28.6, 33.1, 47.5, 56.3°) became apparent and grew shaper. It means that the crystallites of TiO_2 became smaller and the CeO_2 crystallites were formed and growing.

The textual properties of Ce-Ti-O were analyzed by BET method. The surface area, pore volume, and pore diameter are summarized in Table 1. The surface area of TiO_2 and CeO_2 was 21 and 41 m^2/g, respectively. The surface area of all the CeO_2-TiO_2 catalysts was higher than pure TiO_2 since cerium can inhibit the agglomeration of the TiO_2 crystallites. The surface area increased up to 126 m^2/g when ceria content increased to 25% for CeO_2-TiO_2 (1/3). However, the surface area decreased as the Ce content increased from

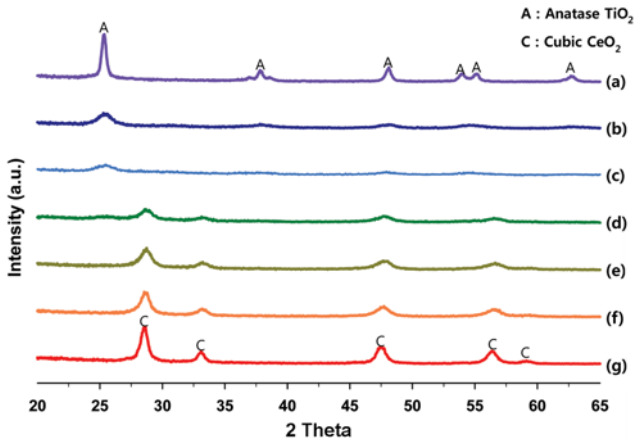

Fig. 1. XRD patterns for (a) TiO_2, (b) Ce/Ti=1/5, (c) Ce/Ti=1/3, (d) Ce/Ti=1/1, (e) Ce/Ti=3/1, (f) Ce/Ti=5/1 (g) CeO_2.

Table 1. Specific surface area (S_{BET}), total pore volume (V_P), and average pore size (D_P) of samples

Catalyst	S_{BET} (m^2/g)	V_P (cm^3/g)	D_P (nm)
TiO_2	21	0.052	97.3
CeO_2-TiO_2 (1/5)	101	0.204	80.7
CeO_2-TiO_2 (1/3)	126	0.292	93
CeO_2-TiO_2 (1/1)	63	0.135	72.2
CeO_2-TiO_2 (3/1)	52	0.169	131.3
CeO_2-TiO_2 (5/1)	49	0.161	128.8
CeO_2	41	0.177	174.2

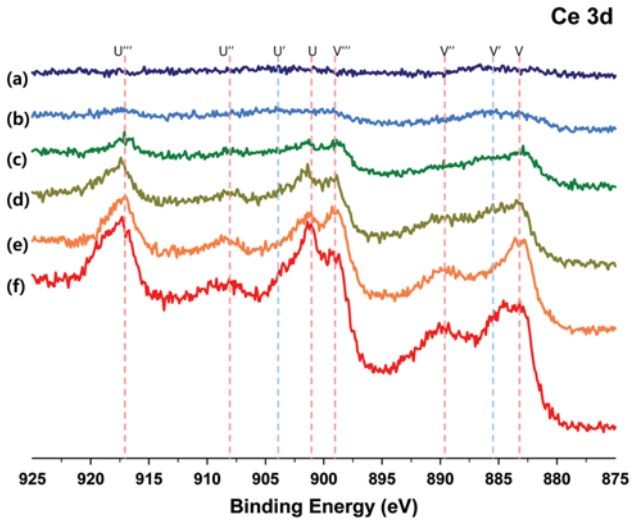

Fig. 2. XPS Ce 3d spectra for (a) Ce/Ti=1/5, (b) Ce/Ti=1/3, (c) Ce/Ti=1/1, (d) Ce/Ti=3/1, (e) Ce/Ti=5/1 (f) CeO_2. The symbols v and u indicate the spin-orbit coupling $3d_{5/2}$ and $3d_{3/2}$, respectively.

25% for CeO_2-TiO_2 (1/3) to 83.3% for CeO_2-TiO_2 (5/1). This was ascribed to the growth of CeO_2 crystallites.

XPS analysis was performed to understand the chemical state of all elements on the catalyst surface. Fig. 2 shows Ce 3d XPS spectra of the fresh CeO_2-TiO_2 catalysts. Ce 3d spectra are very complicated. The labels used in identifying Ce 3d XPS peaks in Fig. 2 were established by Burroughs et al. [36], where v and u indicate the spin-orbit coupling $3d_{5/2}$ and $3d_{3/2}$, respectively. The peaks referred to as v, v″, and v‴ are contributed by CeO_2, and assigned to a mixture of Ce IV ($3d^94f^2$) O ($2p^4$), Ce IV ($3d^94f^1$) O ($2p^5$) and Ce IV ($3d^94f^0$) O ($2p^6$), respectively. The same peak assignment is applied to u structures. The peak v′ is assigned to Ce III ($3d^94f^1$) O ($2p^6$). Ce 3d spectrum of CeO_2 (Fig. 3(a)) shows six peaks at 917.1, 908.2, 901.0, 898.0, 888.9, and 882.9 eV. These peaks represent the presence of Ce^{4+}. The intensity of these six peaks gradually decreased with the increase of Ti concentration. However, the intensity at 903.9 and 885.4 eV slightly increased with the increase of Ti content. These changes in the Ce 3d XPS spectra point to the increase of Ce^{3+} concentration of total Ce in oxides with increasing Ti concentration.

Fig. 3 shows the Ti $2p_{1/2}$ and Ti $2p_{3/2}$ spectra of TiO_2-CeO_2 mixed oxides. The Ti $2p_{3/2}$ peaks were observed at about 458.3-458.8 eV

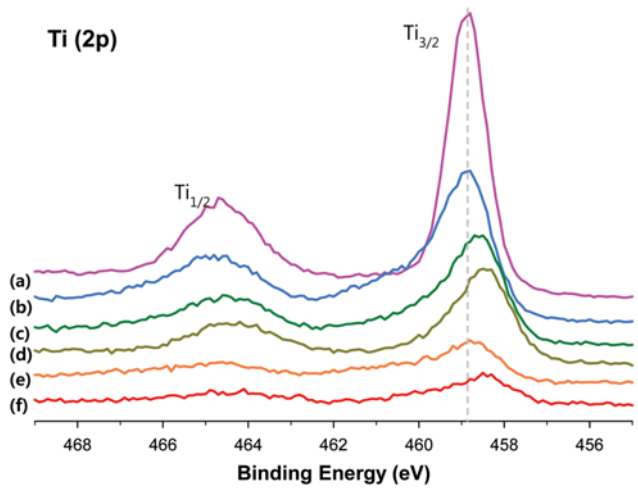

Fig. 3. XPS Ti 2p spectra for (a) TiO_2, (b) Ce/Ti=1/5, (c) Ce/Ti=1/3, (d) Ce/Ti=1/1, (e) Ce/Ti=3/1, (f) Ce/Ti=5/1.

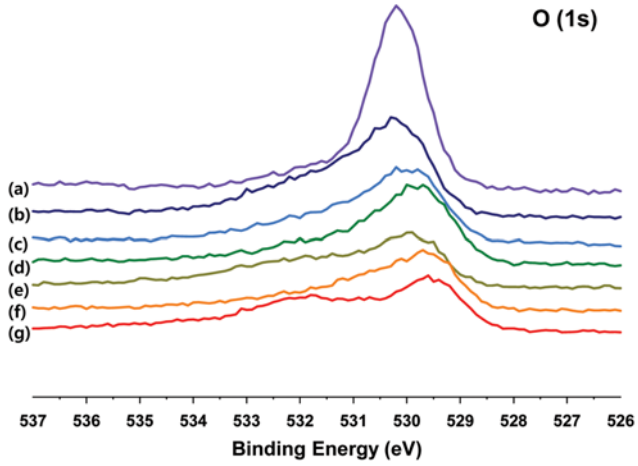

Fig. 4. XPS O 1s spectra for (a) TiO_2, (b) Ce/Ti=1/5, (c) Ce/Ti=1/3, (d) Ce/Ti=1/1, (e) Ce/Ti=3/1, (f) Ce/Ti=5/1 (g) CeO_2.

for TiO_2 and CeO_2-TiO_2 catalysts. The result indicates that Ti is present as TiO_2 on the surface of CeO_2-TiO_2 catalysts [35].

O 1s spectra are shown in Fig. 4; O 1s peaks corresponding to TiO_2 and CeO_2 did not individually appear in the spectra of TiO_2-CeO_2 mixed oxides. Thus, the binding energy of the surface oxygen was sensitive to the concentrations of Ti and Ce in the TiO_2-CeO_2 mixed oxides. This O 1s XPS peak shift suggests that Ti and Ce chemically interact with each other in the TiO_2-CeO_2 mixed oxides. Thus, the mixed oxides are not mixtures of two different oxides but rather a uniform solid solution in which Ti and Ce have chemical interactions [27].

NH_3-TPD profiles of CeO_2-TiO_2 catalysts are shown in Fig. 5. NH_3 desorption of TiO_2, CeO_2 and CeO_2-TiO_2 was observed at 170-680 °C. The NH_3 desorption peaks shifted from 235 to 260, 260, 260, 265, and 270 °C with increasing Ti content; peaks at low temperature (below 300 °C) correspond to weak acid. This desorption temperature of NH_3 suggests that the surface of these oxides is predominantly weakly acidic. In addition, some strong acidity

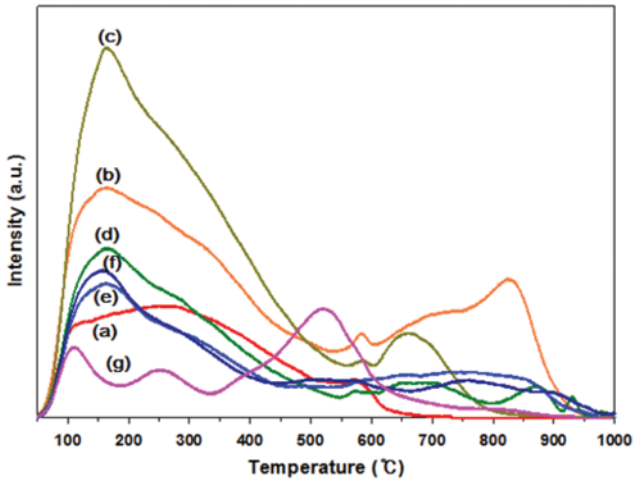

Fig. 5. NH_3-TPD profiles of (a) TiO_2, (b) Ce/Ti=1/5, (c) Ce/Ti=1/3, (d) Ce/Ti=1/1, (e) Ce/Ti=3/1, (f) Ce/Ti=5/1 (g) CeO_2.

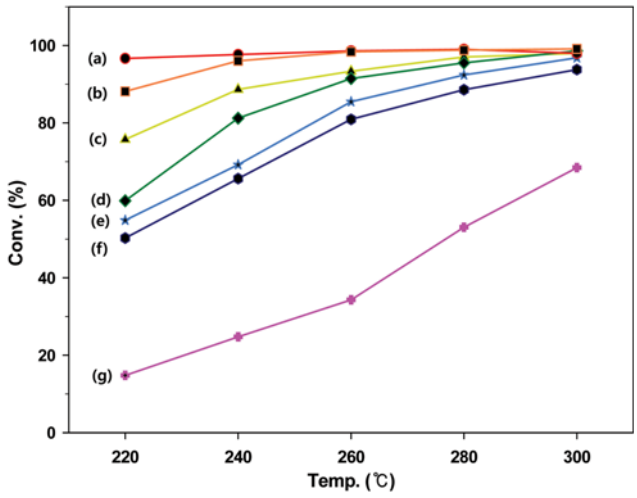

Fig. 7. Conversion of H_2S at different temperatures for (a) Ce/Ti=1/5, (b) Ce/Ti=1/3 (c) Ce/Ti=1/1, (d) TiO_2, (e) Ce/Ti=3/1, (f) Ce/Ti=5/1 (g) CeO_2.

was also identified for the mixed oxides. Mixed oxides catalysts showed lighter amount of strong acid site, which may be attributed to the Lewis acid as reported by Tsyganenko et al. [37].

Fig. 6 presents representative SEM images of the following samples: TiO_2, Ce/Ti=3/1, Ce/Ti=1/3, and Ce/Ti=1/5. In all cases, small and irregular particles of the catalysts were observed. Moreover, from Fig. 6(a), slight aggregates of TiO_2 particles are observed, but better dispersion can be achieved by doping of CeO_2 as shown in Fig. 6(b)-6(d). The emergence of CeO_2 crystals onto the surface of TiO_2 particles can keep two titania globules sufficiently away, thus preventing them from joining together at temperatures at which a pure titania lattice normally sinters [29].

2. Catalytic Performance

Fig. 7 shows the conversion of H_2S using CeO_2-TiO_2 catalysts at the reaction temperature range 220-300 °C, with the reactant com-

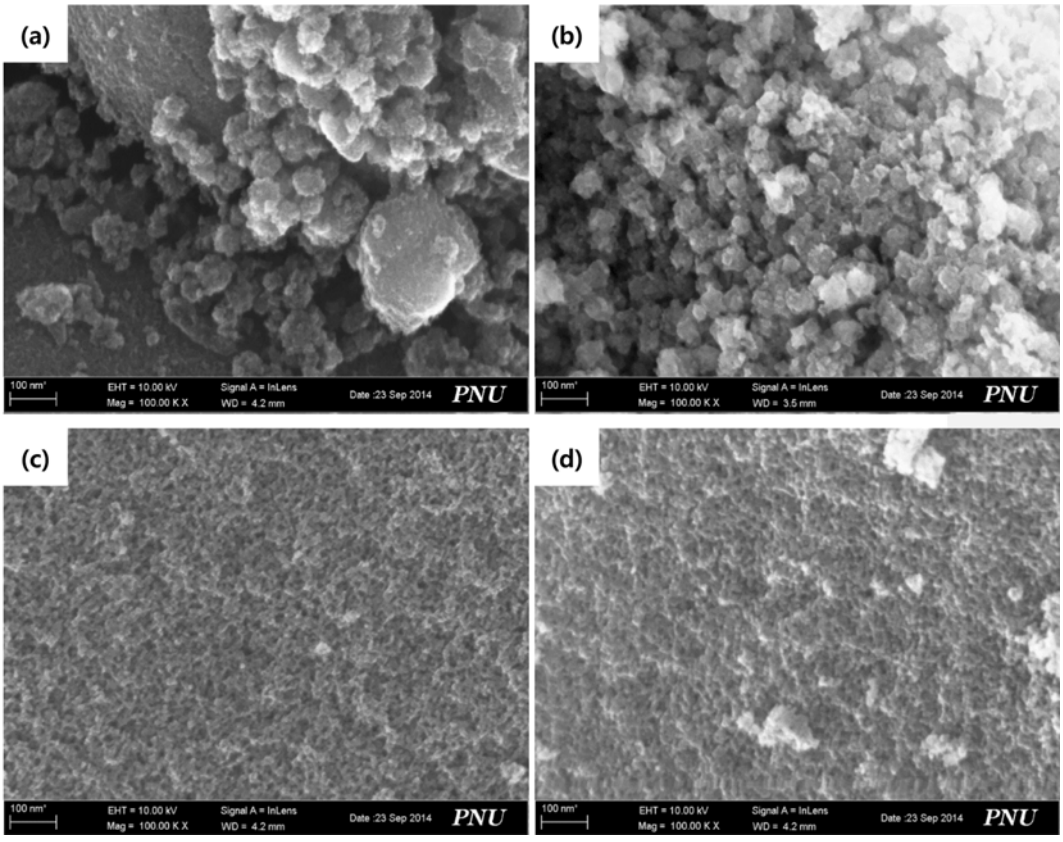

Fig. 6. SEM images for (a) TiO_2, (b) Ce/Ti=3/1, (c) Ce/Ti=1/3, (d) Ce/Ti=1/5.

Table 2. Selectivity to sulfur and SO_2 at different temperatures for CeO_2-TiO_2 with Ce/Ti=1/3

Temp. (°C)	S-S (%)	S-SO_2 (%)
220	99.2	0.8
240	99.0	1.0
260	98.9	1.1
280	98.5	1.5
300	98.2	1.8

Reaction conditions: $H_2S/O_2/He=5/2.5/92.5$, GHSV=10,000 h^{-1}, cat.= 0.5 g, reaction time=1 h

position of $H_2S/O_2/He=5/2.5/92.5$ at GHSV=10,000 h^{-1}. TiO_2 alone showed 60% of H_2S conversion at 220 °C and it increased with temperature and reached to 98.6% at 300 °C probably due to strong acidity of TiO_2. CeO_2 showed the lowest conversion; however, it increased with increasing TiO_2 content in CeO_2-TiO_2. The catalysts of Ce/Ti=1/5 and 1/3 showed very high H_2S conversion near to 100% over 260 °C. This may be due to the presence of high amount of acid sites as observed in the NH_3-TPD (Fig. 5). These catalysts also exhibited high surface area (Table 1) and high amount of Ce^{3+}. With the increase of Ti content, Ce^{3+} increased on the surface of CeO_2-TiO_2 catalysts. The increase of Ce^{3+} content is known to be helpful for the chemisorbed oxygen on the catalyst surface to increase [35]. The catalysts with relatively lower surface area and lower Ce^{3+} content (Ce/Ti=3/1, 5/1) showed lower H_2S conversion. High amount of CeO_2 in the CeO_2-TiO_2 could generate the growth of CeO_2 crystalline, as pointed out by XRD that cubic phase was observed. SEM image of Ce/Ti=3/1 (Fig. 6) also confirmed the growth of CeO_2 crystalline.

Table 2 shows the selectivity of elemental sulfur and sulfur dioxide of CeO_2-TiO_2 catalysts at 220-300 °C. The selectivity of elemental sulfur decreased and the emission of SO_2 increased with temperature.

As mentioned, the elementary reactions (1)-(4) occurred in the Claus process. H_2S is converted to elemental sulfur by reaction (3) and partly to SO_2 by reaction (4). SO_2, which is produced by reactions (1) and (4), can be converted to elemental sulfur by the Claus reaction (2), which has a high selectivity for elemental sulfur. This indicates that the CeO_2-TiO_2 is suitable for catalyzing the industrial oxidation of H_2S to elemental sulfur without considerable SO_2 emission.

CONCLUSIONS

The selective oxidation of H_2S over CeO_2-TiO_2 catalysts was investigated. The synthesized catalysts were analyzed using various physico-chemical characterization techniques. CeO_2-TiO_2 catalysts exhibited excellent conversion of H_2S to elemental sulfur with small amount of SO_2 emission. The conversion of H_2S over CeO_2-TiO_2 catalysts increased when the CeO_2 loading to TiO_2 was up to Ce/Ti=1/3; however, it decreased at higher loadings of CeO_2 because of the formation of crystalline CeO_2. CeO_2-TiO_2 catalysts with Ce/Ti=1/5 and 1/3 exhibited the highest H_2S conversion probably due to the uniform dispersion of metal oxides, high surface area and large amount of acid sites.

ACKNOWLEDGEMENTS

This work was supported by a 2-Year Research Grant of Pusan National University.

REFERENCES

1. B. M. Khudenko, G. M. Gitman and T. E. P. Wechsler, *J. Environ. Eng.*, **119**, 1233 (1993).
2. J. S. Eow, *Environ. Prog. Sustain.*, **21**, 143 (2002).
3. J. A. Lagasm J. Borsboom and P. H. Brben, *Oil Gas J.*, **10**, 68 (1988).
4. R. Ketter and N. Liermann, *Oil Gas J.*, **11**, 63 (1982).
5. R. Kettner, T. Lubcke and N. Liermann, *Eur. Patent*, 0078690 (1983).
6. P. F. M. T. van Nisselrooy and J. A. Lagas, *Catal. Today*, **16**, 263 (1993).
7. J. Borsboom, B. G. Goar, G. Heijkoop and J. A. Lagas, *Sulphur*, **220**, 44 (1992).
8. X. Zhang, Y. Tang, S. Qu, J. Da and Z. Hao, *ACS Catal.*, **5**, 1053 (2015).
9. M. Y. Shin, Ch. M. Nam, D. W. Park and J. S. Chung, *Appl. Catal. A.*, **211**, 213 (2001).
10. K. T. Li and Z. H. Chi, *Appl. Catal. B.*, **31**, 173 (2001).
11. K. T. Li and Z. H. Chi, *Appl. Catal. A.*, **206**, 197 (2001).
12. D. W. Park, B. K. Park, D. K. Park and H. C. Woo, *Appl. Catal. A.*, **223**, 215 (2002).
13. B. G. Kim, W. D. Ju, I. Kim, H. C. Woo and D. W. Park, *Solid State Ion.*, **172**, 135 (2004).
14. M. I. Kim, D. W. Park, S. W. Park, X. Yang, J. S. Choi and D. J. Suh, *Catal. Today*, **111** 212 (2006).
15. K. T. Li and C. H. Huang, *Ind. Eng. Chem. Res.*, **45**, 7096 (2006).
16. K. V. Bineesh, D. R. Cho, S. Y. Kim, B. R. Jermy and D. W. Park, *Catal. Commun.*, **9**, 2040 (2008).
17. K. V. Bineesh, D. K. Kim, M. I. Kim and D. W. Park, *Appl. Clay Sci.*, **53**, 204 (2011).
18. K. V. Bineesh, D. K. Kim, M. I. Kim, M. Selvaraj and D. W. Park, *Dalton Trans.*, **40**, 3938 (2011).
19. K. V. Bineesh, D. K. Kim, D. W. Kim, H. J. Cho and D. W. Park, *Energy Environ. Sci.*, **3**, 302 (2010).
20. K. V. Bineesh, M. I. Kim, M. S. Park, K. Y. Lee and D. W. Park, *Catal. Today*, **175**, 183 (2011).
21. K. V. Bineesh. M. I. Kim, G. H. Lee, M. Selvaraj, K. Hyun and D. W. Park, *J. Ind. Eng. Chem.*, **18**, 1845 (2012).
22. M. I. Kim, G. H. Lee, D. W. Kim, D. H. Kang and D. W. Park, *Korean J. Chem. Eng.*, **31**, 2162 (2104).
23. M. D. Soriano, P. Concepcion, P. Botella and J. M. Lopez Nieto, *Top. Catal.*, **54**, 729 (2011).
24. K. I. Hadjiivanov and D. G. Klissurski, *Chem. Soc. Rev.*, **25**, 61 (1996).
25. M. R. Hoffmann, S. T. Martin, W. Y. Choi and D. W. Bahnemann, *Chem. Rev.*, **95**, 69 (1995).
26. M. Flytzani-Stephanopoulos, T. L. Zhu and Y. Li, *Catal. Today*, **62**, 145 (2000).
27. S. Watamabe, X. Ma and C. Song, *J. Phys. Chem. E.*, **113**, 14249 (2009).

28. Z. M. Shi, W. G. Yu and X. Bayar, *Scr. Mater.*, **50**, 885 (2004).
29. T. Lopez, F. Rojas, R. Alexander-Katz, F. Galindo, A. Balankin and A. Buljan, *J. Solid State Chem.*, **177**, 1873 (2004).
30. S. X. Yang, W. P. Zhu, Z. P. Jiang, Z. X. Chen and J. B. Wang, *Appl. Surf. Sci.*, **252**, 8499 (2006).
31. M. F. Luo, J. Chen, L. S. Chen, J. Q. Lu, Z. C. Feng and C. Li, *Chem. Mater.*, **13**, 197 (2001).
32. K. Josef Antony Raj and B. Viswanathan, *Indian J. Chem. A.*, **49**, 401 (2010).
33. B. Jiang, Z. Wu and Y. Liu, *J. Hazard. Mater.*, **145**, 1249 (2009).
34. X. Gao, Y. Jiang, Y. Zhong, Z. Luo and K. Cen, *J. Hazard. Mater.*, **174**, 734 (2010).
35. S. Yang, W. Zhu, Z. Jiang, Z. Chen and J. Wang, *Appl. Surf. Sci.*, **252**, 8499 (2006).
36. P. Burroughs, A. Hammett, A. F. Orchard and G. Thornton, *J. Chem. Soc., Dalton Trans.*, **17**, 1686 (1976).
37. A. A. Tsyganenko, D. V. Pozdnyakov and V. N. Filimonov, *J. Mol. Struct.*, **29**, 299 (1975).